Bull. Chem. Soc. Ethiop. **2027**, 41(1), 81-97.
DOI: https://dx.doi.org/10.4314/bcse.v41i1.7

ISSN 1011-3924
Printed in Ethiopia
Online ISSN 1726-801X
© 2027 Chemical Society of Ethiopia and The Authors

DESIGN AND SYNTHESIS OF NOVEL *N*-SUBSTITUTED PYRROLE DERIVATIVES AS POTENTIAL ANTIOXIDANT AGENTS: *IN SILICO* AND DFT STUDIES

Nouha Ben Mabrouk[1], Chiraz Youssef [1], Anoir Hfaiedh[2*], Onur Şahin[3], Emine Berrin Poyraz[4], Necmi Dege[4], Walid Elfalleh[5], Hamed Ben Ammar[1]

[1]Laboratory of Heterocyclic Chemistry, Natural Products and Reactivity LR11ES39, Faculty of Sciences of Monastir, University of Monastir, 5019 Monastir, Tunisia
[2]Department of Chemistry, Faculty of Sciences of Monastir, University of Monastir, Avenue of Environment, 5019 Monastir, Tunisia
[3]Department of Occupational Health & Safety, Faculty of Health Sciences, Sinop University, TR-57000 Sinop, Türkiye
[4]Department of Physics, Faculty of Sciences, Ondokuz Mayıs University, TR-5200 Samsun, Türkiye
[5]Department of Biology, College of Science, Imam Mohammad Ibn Saud Islamic University (IMSIU), Riyadh, 11623, Saudi Arabia

(Received March 16, 2026; Revised September 15, 2026; Accepted September 30, 2026)

ABSTRACT. In this work, various aryl-pyrroles **3a-d** were synthesized by condensing different primary amines with 2,5-dimethoxytetrahydrofuran. Then, a Vilsmeier-Haack reaction was performed on the synthesized rings, affording the required formylated derivatives **4a-d** with good yields up to 81%. These compounds were subsequently used to generate a series of new unsaturated α-β alkenes via condensation with two different activated methylenes. Beyond the standard spectroscopic characterization IR, ^{1}H and ^{13}C-NMR spectra, X-ray diffraction analysis was also performed. Alternatively, molecular docking was used to predict and discuss possible interactions between these compounds and the active pockets of the crystal structure of water-forming NADPH Oxidase (PDB: **2CDU**), revealing satisfying features regarding compounds **6a** and **6b**. Finally, additional computational investigations such as DFT computations and ADME profile screening were carried out on the top active compounds to gain some insight into their structure-activity correlations. A safe ADMET profile was predicted, and the relation between their electronic structures and their potential reactive sites was determined.

KEY WORDS: Pyrrole derivatives, Antioxidant activity, Molecular docking, ADMET, DFT

INTRODUCTION

Reactive oxygen species (ROS) are extremely active radicals generated from oxygen molecules, which have an important role in physiological as well as pathological processes [1]. They are produced during cell respiration and can increase significantly under stress circumstances, causing oxidative damage [2]. In fact, oxidative stress plays a major role in the pathophysiology of neurodegenerative illnesses, marked by an imbalance between the generation of ROS and the body's antioxidant defenses, ultimately resulting in neuronal damage and apoptosis [3]. In this context, antioxidant agents mitigate oxidative stress levels by capturing and neutralizing reactive oxygen species (ROS) through electron transfer, converting them into harmless molecules [4]. A variety of synthetic compounds are currently being tested for medicinal purposes. However, these molecules have to cross the blood-brain barrier (BBB) to be effective and act directly on the neurons. Hence, generating antioxidant agents with effective brain cell levels for neuroprotective therapeutics is a crucial problem in biochemical research. During these endeavors, the pyrrole pharmacophore has emerged as both an antioxidant and a neuroprotective agent against

*Corresponding author. E-mail: wbelfallah@imamu.edu.sa
This work is licensed under the Creative Commons Attribution 4.0 International License

superoxide anions, hydroxyl radicals, and DPPH(2,2-diphenyl-1-picrylhydrazyl) radicals [5]. In this prominent array, 1,5-diaryl pyrrole derivatives showed neuroprotective effects against 6-hydroxydopamine (6-OHDA), inhibiting apoptosis and controlling lipid peroxidation in a cellular model of Parkinson's disease (PD) [6]. Similarly, tetrahydrobenzo[*b*] pyrroles and 1,4-dihydroindeno[1,2-*b*]pyrroles were evaluated experimentally using Di-Phenyl Picryl Hydrazyl (DPPH) tests. The results demonstrated that these compounds are efficient antioxidant agents *in vitro*[7]. Similarly, the antioxidant potential of pyrrolo[2,3-b]quinoxaline derivatives was evaluated using DPPH assays, revealing considerable $HO^{\cdot}$ radical scavenging activity in physiological lipid settings [8]. Indeed, Pyrrole-based hydrazide-hydrazones were synthesized and assessed for antioxidant potential. When compared to Trolox, Pyrrole-based hydrazide-hydrazones demonstrated more effective radical scavenging performance, promoting them as lead pharmacophores for generating new antioxidant agents [9].

According to the findings mentioned above, novel pyrrole rings were meticulously synthesized. A formyl group was then introduced into the aryl-pyrrole frameworks via the Vilsmeier reaction, resulting in complex structures with promising pharmacological properties. Furthermore, to enhance their biological potential, Knoevenagel reactions were performed on the aforementioned molecules, providing alkene derivatives. On the other hand, the antioxidant potential of these compounds has been evaluated *in silico* by applying molecular docking as well as using chemoinformatics tools to determine the ADMET profile. Then, the characterization of the structural properties of the novel analogs has been explored theoretically using density functional theory (DFT).

EXPERIMENTAL

Materials and methods

The solvents and chemicals used in all reactions were purchased from commercial suppliers, and they were all used exactly as supplied without any additional purification. All reactions were monitored by TLC coated with neutral (Merck) 60F254 silica gel. Chromatographic columns were performed on Merck silica gel 60 (230-400 Mesh) with the appropriate solvent system(s) reported in the operating mode of the experimental section. The melting points were measured using an Electrothermal 9100 digital melting point apparatus. The IR spectra were recorded with a Bruker Vector 22 spectrometer in the 4000-400 cm^{-1} range. ^{1}H- and ^{13}C-NMR spectra were recorded on a Bruker 300 (75) MHz spectrometer using $CDCl_3$ as a solvent. The spectroscopic data analysis confirms the structures proposed for all the synthesized compounds.

*General procedure for the synthesis of pyrrole derivatives (**3a-d**)*

The reaction was carried out by mixing arylamine **1a-d** (1 mmol) with 2,5-dimethoxytetrahydrofurane **2** (1.302 mmol) and glacial acetic acid (5 mL) in a 25 mL flask heated in an oil bath at 100 °C with stirring for 20 minutes. After cooling at room temperature, the resulting mixture was then poured into ice water and extracted with CH_2Cl_2 (3 x 50 mL). The combined organic layers were dried over $MgSO_4$, then the solvent was removed under reduced pressure to give the desired products **3a-d**.

*5-methyl-3-(1H-pyrrol-1-yl) isoxazole (**3a**).* The product **3a** was obtained as yellow crystals (0.12 g, 82%). m.p.139.8 °C; FT-IR ν(CH_{Ar}): 3100 cm^{-1}, ν(C=C): 1520 cm^{-1}; ^{1}H-NMR (300 MHz, $CDCl_3$) δ (ppm): 7.18 (t, *J*= 2.4 Hz, 2H); 6.36 (t, *J* = 2.4Hz, 2H); 6.11 (s, 1H) and 2.45 (s, 3H). ^{13}C-NMR (75MHz, $CDCl_3$) δ (ppm): 171.4; 159.9; 119.4; 111.8; 94.4 and 13.0.

*2-(1H-pyrrol-1-yl) pyridine (**3b**).* The desired product **3b** was obtained as a brown liquid (0.6g, 78%). ^{1}H-NMR (300 MHz, $CDCl_3$) δ (ppm): 8.43 (dd, J_1 = 4.9 Hz, J_2 = 1.9 Hz, 1H); 7.58-7.67 (m, 3H); 7.26 (d, J = 13.2 Hz, 1H); 7.06 (dd, J_1 = 10.2 Hz, J_2 = 5.7 Hz, 1H) and 6.43 (m, 2H). ^{13}C-NMR (75MHz, $CDCl_3$) δ (ppm): 150.9; 148.1; 137.9; 119.9; 117.6 and 110.9.

*1-p-tolyl-1H-pyrrole (**3c**).* The product **3c** was obtained as a brown solid (0.491g, 67%), m.p.141 °C; FT-IR ν(C=C): 1500cm^{-1}; ^{1}H-NMR (300 MHz, $CDCl_3$) δ (ppm): 7.31-7.33 (m, 4H), 7.24-7.26 (m, 2H), 7.09 (m, 2H), 6.36-6.38 (m, 2H) and 2.41 (s, 3H). ^{13}C-NMR (75MHz, $CDCl_3$) δ (ppm): 138.1; 134.8; 129.5; 120.0; 118.8; 109.5 and 20.2.

*1-(2,6-diisopropylphenyl)-1H-pyrrole (**3d**).* The product **3d** was obtained as a brown solid (0.4 g, 62%). m.p.140 °C; FT-IR ν(CH_{Ar}):3000 cm^{-1};^{1}H-NMR (300 MHz, $CDCl_3$) δ (ppm): 7.40 – 7.45 (m, 1H), 7.25 – 7.28 (m, 2H), 6.68 (td, J_1 = 2.0, J_2 = 0.9 Hz, 2H), 6.36 (td, J_1 = 2.1, J_2 = 0.9 Hz, 2H), 2.51 (hept, J = 6.8 Hz, 2H) and 1.18 (s,12H). ^{13}C-NMR (75MHz, $CDCl_3$) δ (ppm): 146.5; 136.6; 128.3; 122.8; 122.5; 107.7; 27.5 and 24.0.

*General procedure for the synthesis of formyl-pyrrole derivatives (**4a-d**)*

In a 25 mL flask, phosphorus oxychloride (1.322 mmol) was added dropwise to a mixture of dimethylformamide (1.322 mmol) in 4mL of dry CH_2Cl_2 and stirred at 0 °C for 30 minutes. Then the mixture was brought to room temperature with stirring. After 15 minutes, pyrrole derivatives **3a-d** (1mmol) were added and the mixture was cooled again at 0 °C for 30 minutes and then refluxed for 7-8 h at 80 °C. The reaction was monitored by TLC. After cooling at room temperature, the resulting mixture was poured into ice water, and 20 mL of a solution of $NaHCO_3$ was added. The organic layer was extracted with ethyl acetate (2 x 50 mL), dried over $MgSO_4$ then concentrated under reduce pressure to give the appropriate formyl-pyrrole **4a-d**.

*1-(5-methyl-1,2-oxazol-3-yl)-1H-pyrrole-2-carbaldehyde (**4a**).* The product **4a** was obtained as a brown liquid (0.983 g, 81%). ^{1}H-NMR (300 MHz, $CDCl_3$) δ (ppm): 9.67 (s, 1H); 7.28 (dd, J_1 = 2.6 Hz, J_2 = 1.7 Hz, 1H); 7.09 (dd, J_1 = 3.9 Hz, J_2 = 1.7 Hz, 1H); 6.33 (dd, J_1 = 3.9 Hz, J_2 = 2.8 Hz, 1H); 6.30 (s, 1H) and 2.38 (s, 3H). ^{13}C-NMR (75MHz, $CDCl_3$) δ (ppm): 178.4; 170.5; 158.7; 132.0; 129.3; 124.6; 111.3; 98.4 and 12.0.

*1-(pyridin-2-yl)-1H-pyrrole-2-carbaldehyde (**4b**).* The formyl-pyrrole **4b** was collected as a brown solid (0.588 g, 70.33%). m.p.105.3 °C; FT-IR ν(C=O): 1720 cm^{-1}; ^{1}H-NMR (300 MHz, $CDCl_3$) δ (ppm): 9.76 (s, 1H); 8.45-8.48 (m, 1H); 7.73 -7.80 (m, 1H); 7.38-7.43 (m, 2H); 7.25 (ddd, J_1 = 7.6 Hz, J_2 = 5 Hz, J_3 =1.4 Hz, 1H); 7.16 (dd, J_1 = 4.3 Hz, J_2 = 2.1 Hz, 1H) and 6.35 – 6.39 (m, 1H). ^{13}C-NMR (75MHz, $CDCl_3$) δ (ppm): 179.4; 150.9; 148.6; 138.2; 132.3; 129.8; 123.9; 122.6; 118.8 and 111.2.

*1-p-tolyl-1H-pyrrole-2-carbaldehyde (**4c**).* The product **4c** was obtained as a yellow liquid (0.5 g, 51%).^{1}H-NMR (300 MHz, $CDCl_3$) δ (ppm): 9.58 (s, 1H), 7.27 (d, J = 1.9 Hz, 3H), 7.16 (dd, J = 4.0, 1.7 Hz, 1H), 7.06 (t, J = 2.1 Hz, 1H), 6.41 (dd, J = 4.0, 2.5 Hz, 1H) and 2.44 (s, 3H). ^{13}C-NMR (75MHz, $CDCl_3$) δ (ppm): 178.4; 137.7; 135.8; 132.3; 130.4; 129.1; 125.3; 121.0; 110.1; and 20.5.

*1-(2,6-diisopropylphenyl)-1H-pyrrole-2-carbaldehyde (**4d**).* The product **4d** was obtained as a brown solid (0.5g, 62%). m.p.108.5 °C; FT-IR ν(C=O): 1700 cm^{-1}; ^{1}H-NMR (300 MHz, $CDCl_3$) δ (ppm): 9.88 (s, 1H), 7.45 (t, J = 7.7 Hz, 1H), 7.25-7.28 (m, 2H), 6.81 (t, J = 2.2 Hz, 1H), 6.67 (t, J = 2.5 Hz, 1H), 2.45 (hept, J = 6.9 Hz, 2H) and 1.16 (s,12H).

*General procedure for the synthesis of unsaturated α-β nitriles (**5a-d**)*

Formylpyrroles **4a-d** (1 mmol) were mixed with malononitrile (1 mmol) and a few drops of Et_3N in 3 mL of dry ethanol. The resulting mixture was stirred at room temperature for 5-10 minutes, then the crude product was collected by filtration, washed with hexane, and dried under vacuum to afford the unsaturated α-β-nitriles **5a-d**.

*[1-(5-methyl-1,2-oxazol-3-yl)-1H-pyrrol-2-yl]methylidene propanedinitrile (**5a**).* The product **5a** was collected as a brown solid (0.273g, 70%). m.p. 140 °C; FT-IR ν(CN): 2227 cm^{-1}, ν(C=CH): 1575 cm^{-1}; ^{1}H-NMR (300 MHz, $CDCl_3$) δ (ppm): 8.25 (s, 1H); 7.86 (dd, J_1 = 4.3 Hz, J_2 = 1.4 Hz, 1H); 7.31 – 7.33 (m, 1H); 6.63 (dd, J_1 = 4.3 Hz, J_2 = 2.8 Hz,1H); 6.19 (s, 1H); and 2.56 (s, 3H). ^{13}C-NMR (75 MHz, $CDCl_3$) δ (ppm): 170.2; 155.8; 143.0; 126.9; 124.9; 119.4; 112.1; 112.0; 111.3; 94.9 and 10.2.

*[1-(pyridin-2-yl)-1H-pyrrol-2-yl]methylidene propanedinitrile (**5b**).* The crude product **5b** was obtained as a yellow solid (0.110 g, 85.93%). m.p. 125.4 °C; FT-IR ν(CH_{Ar}): 3000 cm^{-1},ν(CN): 2300 cm^{-1}, ν(C=CH): 1525 cm^{-1}; ^{1}H-NMR (300 MHz, $CDCl_3$) δ (ppm): 8.63 – 8.65 (m, 1H), 8.14 (s, 1H), 7.95 (td, *J* = 7.8, 1.9 Hz, 1H), 7.88 (d, *J* = 4.3 Hz, 1H), 7.41 – 7.47 (m, 2H), 7.35 (d, *J* = 8.0 Hz, 1H) and 6.60 – 6.63 (m, 1H).^{13}C-NMR (75 MHz, $CDCl_3$) δ (ppm): 150.6; 149.5; 146.5; 139.4; 129.9; 123.2; 121.5; 118.4; 115.1; 114.0 and 113.6.

*2-((1-p-tolyl-1H-pyrrol-2-yl)methylene)malononitrile (**5c**).* The product **5c** was collected as a green liquid (0,019 g, 50%).^{1}H-NMR (300 MHz, $CDCl_3$) δ (ppm): 7.72 (s, 1H), 7.28 (d, *J* = 8.1 Hz, 2H), 7.18 (d, *J* = 4.2 Hz, 2H), 7.15 (dd, *J* = 2.6, 1.4 Hz, 1H), 7.08 (t, *J* = 8.4 Hz, 3H), 6.48 (dd, *J* = 4.5, 2.5 Hz, 1H) and 3.50 (s, 3H).^{13}C-NMR (75MHz, $CDCl_3$) δ (ppm): 144.7; 139.9; 132.1; 130.4; 130.3; 126.6; 126.2; 124.3; 120.1; 115.1; 114.0; 113.3 and 29.6.

*2-((1-(2,6-diisopropylphenyl)-1H-pyrrol-2-yl)methylene)malononitrile (**5d**).* The crude product **5d** was obtained as a brown liquid (0.018g, 51%).^{1}H-NMR (300 MHz, $CDCl_3$) δ (ppm): 7.61 (s, 1H), 7.34– 7.40 (m, 1H), 7.26 (d, *J* = 1.9 Hz, 1H), 7.17 – 7.19 (m, 2H), 6.99 (dd, *J* = 3.1, 1.8 Hz, 1H), 6.67 (dd, *J* = 3.1, 2.0 Hz, 1H), 2.24 – 2.33 (m, 2H), 1.07 (dd, *J* = 6.9, 0.9 Hz, 12H). ^{13}C-NMR (75 MHz, $CDCl_3$) δ (ppm): 153.2; 145.9; 134.9; 131.2; 130.1; 127.2; 123.9; 119.2; 110.1; 28.3 and 24.3.

*General procedure for the Synthesis of unsaturated compounds (**6a-d**)*

A mixture of formylpyrrole derivatives **4a-d** (1 mmol) with 3-methyl-1-phenyl-1*H*-pyrazol-5(4*H*)-one (1 mmol) was stirred at room temperature in the presence of a few drops of triethylamine in 3 mL of dry ethanol for 24 h. An extraction with dichloromethane was performed, followed by evaporation of the solvent to give the desired products **6a-d**.

*3-methyl-4-((1-(5-methylisoxazol-3-yl)-1H-pyrrol-2-yl)methylene)-1-phenyl-1H-pyrazol-5(4H)-one (**6a**).* The product **6a** was collected as an orange crystal (0.106 g, 28%). m.p.179.3°C; FT-IR ν(C=CH): 1525 cm^{-1}; ^{1}H-NMR (300 MHz, $CDCl_3$) δ (ppm): 8.85-8.87 (m, 1H); 7.89-7.94 (m, 2H); 7.33 (dd, J_1 = 4.2 Hz, J_2 = 2.9 Hz, 2H); 7.22 (dd, J_1 = 2.8 Hz, J_2 = 1.5Hz, 1H); 7.05 – 7.12 (m, 1H); 6.52(dd, J_1 = 4.2 Hz, J_2 = 2.9Hz, 1H); 6.11 (s, 1H); 2.46 (s, 3H) and 2.22 (s, 3H). ^{13}C-NMR (75 MHz, $CDCl_3$) δ (ppm): 131.1; 129.4; 129.3; 128.6; 126.8; 124.4; 119.0; 113.9; 97.6; 29.6 and 12.6.

*3-methyl-1-phenyl-4-((1-(pyridin-2-yl)-1H-pyrrol-2-yl)methylene)-1H-pyrazol-5(4H)-one (**6b**).* The product **6b** (0.097g, 51%) was obtained as a brown liquid. ^{1}H-NMR (300 MHz, $CDCl_3$) δ

(ppm): 9.69 (s,1H); 8.40-8.43 (m, 1H); 7.68-7.75 (m, 1H); 7.33 – 7.37 (m, 2H); 7.16 – 7.22 (m, 1H); 7.08 – 7.11 (m, 1H); 6.31-6.34 (m, 1H); 1.18 (s, 3H).^{13}C-NMR (75 MHz, $CDCl_3$) δ (ppm):179.3; 148.6; 138.2; 130.0; 124.2; 122.6; 119.0; 111.2 and 29.6.

*4-((1-(2,6-diisopropylphenyl)-1H-pyrrol-2-yl)methylene)-3-methyl-1-phenyl-1H-pyrazol-5(4H)-one (**6d**).* The product **6d** (0.030g, 62%) was collected as a yellow solid. m.p.174.1°C; FT-IR ν(C=CH): 1500cm^{-1}; ^{1}H-NMR (300 MHz, $CDCl_3$) δ (ppm): 8.50 (s, 1H), 7.86 – 7.90 (m, 2H), 7.27 – 7.37 (m, 4H), 7.16 (d, J = 7.7 Hz, 3H), 7.02 – 7.08 (m, 2H), 6.65 (dd, J_1 = 2.9, J_2 = 2.0 Hz, 1H), 2.33 – 2.45 (m, 2H), 2.27 (s, 3H), 1.10 (s, 3H), 1.08 (d, J = 1.5 Hz, 6H), 1.06 (s, 3H). ^{13}C-NMR (75MHz, $CDCl_3$) δ (ppm): 185.4; 162.8; 150.3; 146.1; 139.5; 138.9; 135.8; 134.0; 129.7; 129.6; 128.6; 125.6; 124.3; 123.7; 123.7; 121.5; 120.3; 119.1; 114.8; 28.3; 24.4 and 13.0.

X-ray diffraction analysis

Suitable crystals of compounds were selected for data collection, which was performed on a D8-QUEST diffractometer equipped with a graphite-monochromated Mo-K_α radiation at 293 K. The structures were solved by direct methods using SHELXS-2013 [10] and refined by full-matrix least-squares methods on F^2 using SHELXL-2013 [11]. The H atoms were located from different maps and then treated as riding atoms with C-H distances of 0.93-0.98 Å. The large s.u. values and displacement parameters of some atoms are caused by the disorder. The refinements of the disordered groups were made anisotropicaly using PART and DFIX restrictions These disorders were modelled as two different orientations as two groups [first group= C1, C2, C3 and second group = C1A, C2A, C3A for **6a**; first group= C1A, C2A, C3A, C4A, C5A, O1A and second group = C1B, C2B, C3B, C4B, C5B, O1B for **4d**], with occupancy factors of 0.503(5) and 0.497(5) for **6a** and 0.380(11) and 0.620(11) for **4d**, respectively. The following procedures were implemented in our analysis: data collection: Bruker APEX3[12]; programs used for molecular graphics were as follows: MERCURY programs [13]; GUI for other software related to structure solution: WinGX [14]. Details of data collection and crystal structure determinations are given in Table S5 (supporting information). Crystallographic data (a 7.6764(19) b 10.439(3) c 11.225(3) P-1) for **6a** and (a 17.035(5) b 17.035(5) c 28.486(9) R3c) for **4d** have been deposited with the Cambridge Crystallographic Data Centre under the name of data_shelx with a supplementary publication number CCDC of 2420575 and 2478473, respectively. Copies of the data can be obtained, free of charge, on application to CCDC, 12 Union Road, Cambridge CB2 1EZ, UK.

Molecular docking procedure

The molecular docking simulations were executed utilizing the AutoDock 1.5 software tools [15]. The 3D molecular structures of the synthesized compounds were designed using ACD (3D viewer) software. The target structure in the PDB was identified through the RCSB Protein Data Bank (https://www.rcsb.org/). First, the water molecules were removed, and the hydrogens that were absent were introduced into the system as part of the receptor input file preparation process. After that, AutoDock Tools were employed to generate the PDBQT files containing the ligands and proteins, respectively. Subsequently, the docking calculation was carried out using AutoDock Vina. Finally, the interactions were subsequently visualized and analyzed using the BIOVIA Discovery Studio 2017 R2 (DSV).

ADMET proprieties

To predict the pharmacokinetic characteristics of all synthesized compounds, including molecular weight, number of hydrogen-bond acceptors, number of hydrogen-bond donors, number of rotatable bonds, topological polar surface area, molecular volume, Lipinski Rule, and Pfizer Rule,

the online server Suiss Adme (http://www.swissadme.ch/) and ADMET lab 2.0 (https://admetmesh.scbdd.com/).

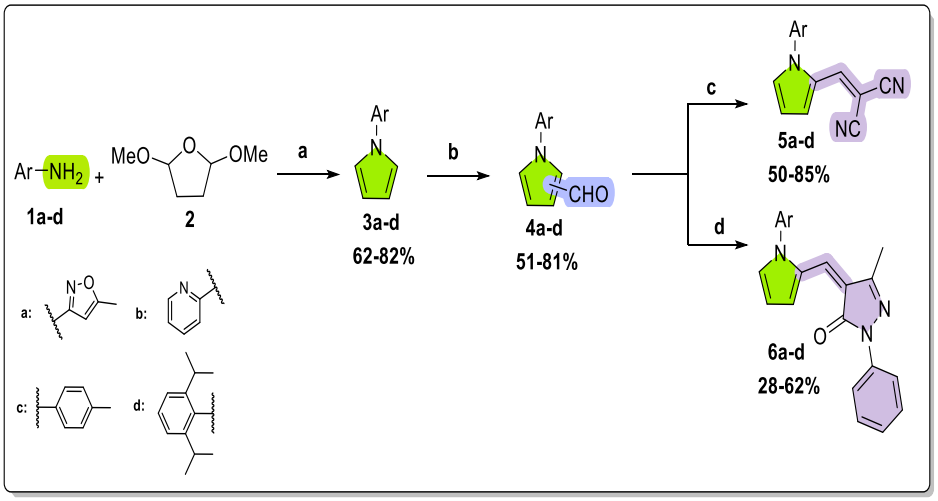
DFT studies

The DFT calculations were executed utilizing GAUSSIAN 09 [16] and GaussView 5.0 [17]. The optimization of the ground-state molecular structures of compounds is achieved through the utilization of the B3LYP/6-311G(d,p) level of theory. The molecular stability and reactivity are assessed through the utilization of the gap energy, which is defined as the difference between the HOMO and LUMO orbitals.

RESULTS AND DISCUSSION

Chemistry

Several studies have meticulously examined the potential of pyrrole derivatives as efficient antioxidants, pointing out their capacity to reduce oxidative stress via free radical scavenging processes [18-20]. The elucidation of structure-activity relationships conveys crucial information about the molecular factors responsible for their antioxidative capabilities. These insights lay a robust foundation for developing a rational structure of pyrrole compounds with improved pharmacological features. Along the same path, many researchers have focused their work on the synthesis of the pyrrole ring [21, 22] especially through applying the Clauson-Kass reaction [23, 24]. With this aim, we synthesized novel *N*-substituted pyrroles **3a-d** via protecting various arylamines 1a-d with 2,5-dimethoxytetrahydrofuran **2** in acetic acid (Scheme 1). In fact, the FTIR spectra revealed a characteristic υ(C =C_{Ar}) vibration band, which was observed in the range of 2800cm^{-1} confirming the formation of the pyrrole cycle in all synthesized complexes **3a-d**. Indeed, the ^{1}H-NMR spectra indicated the presence of 3 characteristic signals ranging from 6.11 to 7.80 ppm, indicating the formation of the pyrrole cycle.



Scheme 1. Synthetic pathway of pyrrole derivatives. Reagents and conditions: **a**: glacial AcOH, 100 °C, 20 min; **b**: $POCl_3$, DMF, CH_2Cl_2, 80 °C, 7h; **c**: malononitrile, Et_3N, EtOH, rt, 10min; **d**: $C_{10}H_{10}N_2O$, Et_3N, EtOH,rt, 24h.

The latter formylpyrroles intermediates **4a-d** were synthesized following the classical Vilsmeier approach [25]. We mixed DMF with $POCl_3$ in anhydrous CH_2Cl_2 at 0°C for 30 min to form the iminium salt. Then, pyrrole derivatives **3a-d** were added to the reactive medium, and the reaction was carried out at 80 °C for 7 h. The products obtained with moderate to high yields were characterized by NMR spectroscopy, which revealed the presence of a signal in the range of 9.58 to 9.88 ppm corresponding to the proton of the aldehyde function. In this case, the formyl group expands the pyrrole ring's π-conjugation system, resulting in stronger electron delocalization. This change not only maintains the stability of the molecule, but also adjusts its electronic proprieties, making it more reactive toward certain biological targets.

Our focal point was to further enhance the biological potential by increasing the conjugated system; thus, we applied the Knoevenagel reaction [26] on the formylated pyrroles **4a-d** to create novel alkenes bearing pyrrole moieties. Firstly, we condensed the formylpyrroles **4a-d** with malononitrile in dry ethanol and in the presence of a catalytic amount of triethylamine. This reaction was stirred at room temperature for 10min to give unsaturated α-β nitriles **5a-d** with high yields up to 85%. Then, the same process was applied by changing the activated methylene to 3-methyl-1-phenyl-1*H*-pyrazol-5(4H)-one, giving the desired products **6a-d** with moderate yields. All those compounds were then characterized by IR and NMR spectroscopy, in which we observed the presence of a characteristic bond related to the ν (C=CH) stretch, which appeared in 1525-1575cm^{-1}. Additionally, the ^{1}HNMR spectra indicated the presence of a signal related to the proton of the alkene function, which indicates the formation of the desired compounds.

Crystal structure description

The molecular structure of the compounds **4d** and **6a**, with the atom numbering schemes, is shown in Figure 1, in which the displacement ellipsoids of non-H atoms are drawn at the 50% probability level.

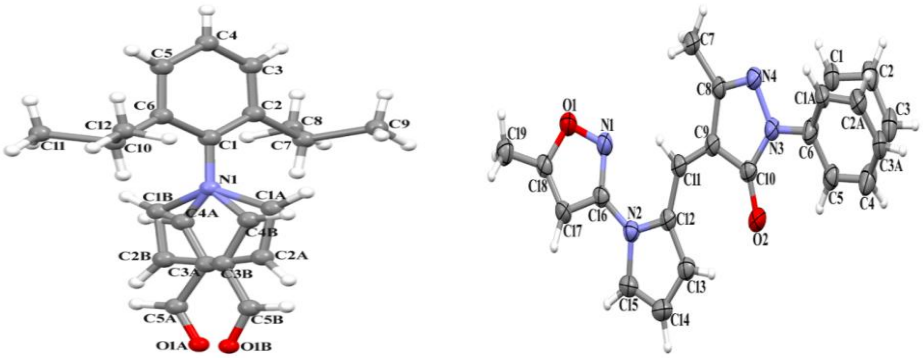


Figure 1. The molecular structure of **4d** and **6a** showing the atom numbering schemes.

The C5-O1 [1.192 (10) Å and 1.201 (11) Å] in **4d** and C10-O2 [1.222 (4) Å**]** in **6a** bond distances are typical of double-bond character (Table S1).

For **6a**, the isoxazole, pyrrole, and pyrazole groups of the ligand are planar, and the dihedral angle between each pair of neighboring planes is 24.55(2)° in (Py(N1)-Py(N2)), 3.37(2)° in (Py(N2)-Py(N3)), and 22.70(2)° in (Py(N1)-Py(N3)), respectively. Additionally, its molecules are

linked by a combination of C-H···O hydrogen bonds (Table 1), C-H···π and π···π interactions (Table 2). Those related to **4d** are linked by a combination of C-H·π interactions.

Table 1. Hydrogen-bond parameters for **6a** (Å, º).

D-H· · ·A	D-H	H···A	D···A	D-H···A
6a				
C11—H11···N1	0.93	2.29	2.956 (5)	129
C13—H13···O2	0.93	2.21	2.946 (5)	136
C5—H5···O2	0.93	2.28	2.906 (5)	124
C19—H19*B*···O2^{i}	0.96	2.47	3.250 (5)	138

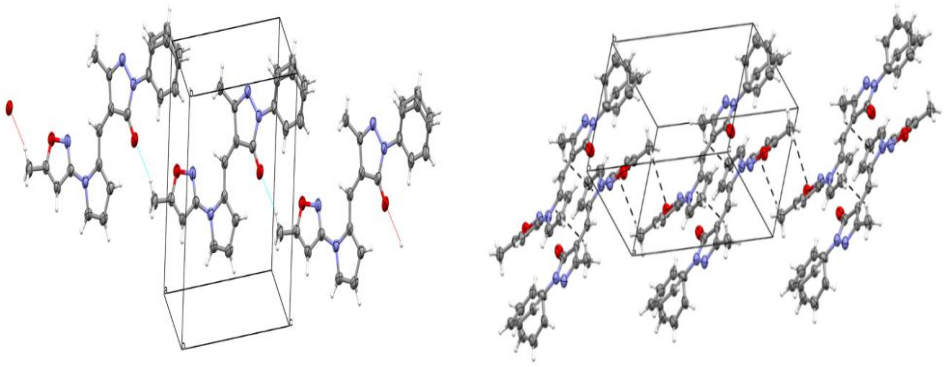
Symmetry code: (i) *x*+1, *y*, *z*−1 for **6a**.

Table 2. C-H···π and π···π interaction parameters (Å, °).

D-H···Cg	D-H	H···Cg	D···Cg	D-H···Cg
6a				
C7-H7C···Cg(2)^{i}	0.96	2.89	3.682 (1)	140
C19-H19B···Cg(1)^{ii}	0.96	2.95	3.623 (1)	128
4d				
C2B-H2B···Cg(3)^{i}	0.93	3.00	3.750 (1)	139
C5B-H5B···Cg(3)^{ii}	0.93	2.89	3.814 (1)	173
C7-H7···Cg(1)	0.98	2.89	3.641 (1)	134
C7-H7···Cg(2)	0.98	2.77	3.534 (1)	135
C10-H10···Cg(1)	0.98	2.79	3.556 (1)	135
C10-H10···Cg(2)	0.98	2.93	3.674 (1)	134
C2A-H2A···Cg(3)^{ii}	0.93	2.91	3.679 (1)	140
C5A-5A···Cg(3)^{i}	0.93	2.89	3.815 (1)	172
Cg(I)	Cg(J)		Cg-Cg	Perpendicular distance
6a				
Cg(2)	Cg(3)^{iii}		3.647	3.512

Symmetry codes: (i) 2-x, 1-y, 1-z; (ii) 2-x, 1-y, -z: (iii) 1-x, 1-y, 1-z; Cg(1)=O1/N1/C16/C17/C18; Cg(2)=N2/C12/C13/C14/C15; Cg(3)=N3/N4/C8/C9/C10 for **6a**; (i) 1/3-x+y, -1/3+y, 1/6+z; (ii) 2/3-y, 1/3-x, -1/6+z; Cg(1)=N1/C1B/C2B/C3B/C4B; Cg(2)=N1/C1A/C2A/C3A/C4A; Cg(3)=C1-C6 for **4d.**

Otherwise, the C19 atom, for **6a**, acts as a hydrogen bond donor to the O2^{i} atoms, forming a C(11) chain (Figure 2) running which is parallel to the (101) direction ((i) x+1, y, z-1). Otherwise, the C7 atom in the molecule at (x, y, z) acts as a hydrogen-bond donor to the pyrrole ring in the molecule at (2-x, 1-y, 1-z), forming a centrosymmetric $R_2^2(14)$ ring centered at (1, 1/2, 1/2). Similarly, the C19 atom in the molecule at (x, y, z) acts as a hydrogen-bond donor to the isoxazole ring in the molecule at (2-x, 1-y, -z), forming a centrosymmetric $R_2^2(8)$ ring centered at (1, 1/2, 0). The combination of these C-H···π interactions produces edge-fused $R_2^2(8)R_2^2(14)$ rings along (001) direction.



A B

Figure 2. A: The formation of C(11) chain along (101) direction in **6a** and B: The formation of edge-fused R22(8)R22(14) rings along (001) generated by C-H···π interactions in **6a**.

In **4d**, the C-H···π interactions contribute to a three-dimensional supramolecular network (Figure S1, supporting information).

Molecular docking study

NADPH oxidase (NO) represents a category of enzymes that convert electrons to oxygen molecules and lay a robust foundation for the generation of reactive oxygen species (ROS) [27]. It is known as the key enzyme responsible for producing ROS during the metabolism of arachidonic acid, which leads to harmful oxidative stress contributing to neuronal degeneration.

The inhibition of NO interrupts and blocks the ROS production cycle, which leads to reduced oxidative stress and restoration of redox homeostasis [28]. In this context, several studies have been directed towards *in silico* studies to better understand the interaction modes of drugs with free-radical scavenging activities in the active site of NO [29, 30]. With this aim, we performed molecular docking on the synthesized compounds and tested their antioxidant potential toward the crystal structure of water-forming NADPH oxidase from *Lactobacillus sanfranciscensis* (PDB: 2CDU). All the selected compounds were inserted into the same active pocket of the target protein (B chain) and interacted with the same key amino acid residues [31] as well as the co-crystallized ligand (adenosine-5'-diphosphate), which was re-docked while maintaining the same parameters.

All the hydrogen bond and hydrophobic interactions of each ligand within the different amino acids of the receptor protein, as well as the energy scores of the docked conformations, are detailed in Table 3. Energy scores ranging between -6.1 and -5.2 were presented for pyrrole rings **3a-d**, in which 5-methyl-3-(1H-pyrrol-1-yl) isoxazole **3a** is the most stable compound with the lowest energy (-6.1), presenting one hydrogen bond with ASP282 due to the presence of the isoxazole ring. Otherwise, the incorporation of the formyl group into pyrrole derivatives increases the energy scores of these compounds, which may exhibit higher activity. This is demonstrated by the energy scores, which fluctuated between -6.7 and -6.3, in which **4a**, **4b**, and **4c** presented 3 hydrogen bonds with THR9, ALA11, and GLY12, and **4d** presented one hydrogen bond with GLY43 along with 13 hydrophobic interactions with different amino acid residues. Similarly, the α-ß unsaturated system has an influence on the biological potential of the formylpyrroles **4a-d**. In fact, the improvement of the conjugated system with 2 nitrile groups increases the energy scores of the unsaturated α-ß nitriles **5a-d**, which ranged from -7.7 to -7.2. However, the aromatic 3-methyl-1-phenyl-1H-pyrazol-5(4H)-one had more influence on the biological potential, which

increased the energy scores of **6a-d** from -9.8 to -7.8. Thus, we observed that among these docked complexes, the compounds **6a** and **6b** have shown energy scores of -9.8 and -8.7, respectively, which were lower than Adenosine-5'-diphosphate, the reference ligand (-8.1). Indeed, (3-methyl-4-((1-(5-methylisoxazol-3-yl)-1*H*-pyrrol-2-yl)methylene)-1-phenyl-1*H*-pyrazol-5(4*H*)-one) **6a** illustrated 3 hydrogen bonds along with 15 interactions with amino acid residues. In fact, two hydrogen bonds were depicted between the non-bonding doublet of the oxygen and nitrogen of the oxazole ring with CYS8 and THR9 residues, respectively, and one bond was presented between the nitrogen of the pyrazole ring and SER41. Likely, 3-methyl-1-phenyl-4-((1-(pyridin-2-yl)-1*H*-pyrrol-2-yl)methylene)-1*H*-pyrazol-5(4*H*)-one **6b** showed 2 hydrogen bonds between the nitrogen of the pyridine ring and the pyrazole ring with THR9 and SER41, along with 15 other interactions with different amino acid residues. Hence, according to these findings, we can assume that compounds **6a** and **6b** may serve as antioxidant agents due to their ability to form stable ligand-protein complexes. Therefore, they were selected for subsequent ADMET and DFT analyses.

Table 3. Molecular docking results of the synthesized compounds.

Ligand	Energy kcal mol^{-1}	Interactions with amino acids	
		H-bond interactions	Hydrophobic interactions
3a	-6.1	ASP282*	THR9*, HIS10*, ALA11*, GLY12*, SER41*, THR112*, GLY114*, LYS134*, GLY281*, ASP282*, SER283*.
3b	-5.2	-	THR9*, HIS10**, ALA11*, SER41*, GLY114*, GLY281*, ASP282*, LEU299* ALA300*, ALA303*.
3c	-5.9	-	VAL6*, GLY7*, TYR31*, GLU32*, MET33**, VAL81*, GLY80*, THR113*, ASN248*, GLN250*, LEU251*.
3d	-5.3	-	THR9*, HIS10*, ALA11*, PHE39*, SER41*, THR113*, GLY114*, SER115*, ASN135*, GLY281*, ASP282*, ALA303*.
4a	-6.7	THR9*, ALA11*, GLY12*	GLY7, CYS8*, THR9*, HIS10*, THR13*, THR112*, THR113*, GLY114*, SER115*, LYS134*, GLY281*, ASP282*, LEU299*, ALA300*, ALA303*.
4b	-6.4	THR9*, ALA11*, GLY12*	THR9*, HIS10*, THR112*, THR113*, GLY114*, SER115*, LYS134*, ASP282*, ALA300*, ALA303*.
4c	-6.7	THR9*, ALA11*, GLY12*	THR9*, ALA11*, ASN34*, THR112*, THR113*, GLY114*, SER115*, LYS134**, ASN135*, GLY281*, ASP282*, ALA303*.
4d	-6.3	GLY43*	LEU40*, SER41*, ILE44*, ALA45*, CYS133*, LYS134*, TYR159*, ILE160***, GLU163*, LEU164*, PHE245*.
5a	-7.5	HIS10*, ALA11*	THR9*, ALA11*, GLY12*, PHE39*, LEU40*, SER41*, THR112*, GLY114*, LYS134*, ASN135*, GLY281*, LEU299*, ALA300*, ALA303**.
5b	-7.2	ASN34*	GLY7*, CYS8*, THR9*, HIS10*, ALA11*, GLY12*, GLU32*, ASN36*, PHE39*, SER41*, THR112*, THR113*, GLY114*, SER115*, LYS134*, ASN135*, TYR136*, ASN248*.
5c	-7.2	ASN248*	VAL6*, GLY7*, CYS8*, THR9*, GLU32*, MET33**, ASN34*, GLN80*, VAL81*,

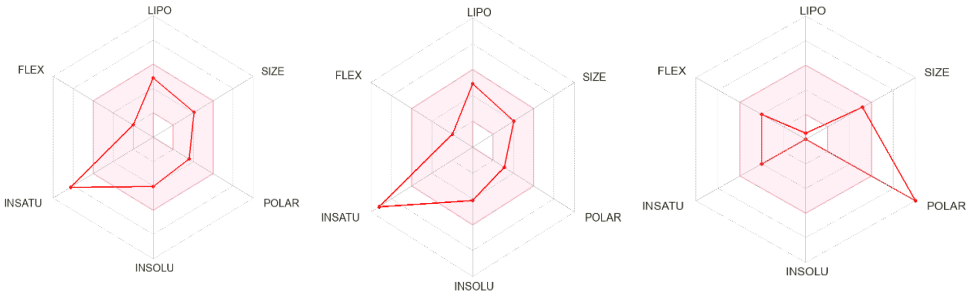
			THR112*, THR113*, SER115*, LYS116*, LEU251*.
5d	-7.7	SER41*, ALA300*	HIS10*, LEU40*, GLY43*, ILE44*, ALA45*, CYS133*, LYS134*, ILE160***, GLU163*, PHE245**, LEU299*.
6a	-9.8	CYS8*, THR9*, SER41*	GLY7*, THR9*, HIS10*, ALA11*, GLY12*, GLU32*, THR112*, THR113*, GLY114*, LYS134*, ILE160*, PHE245*, GLY281*, ASP282*, ALA303*.
6b	-8.7	THR9*, SER41*	GLY7*, CYS8*, THR9*, HIS10*, ALA11*, THR112*, THR113*, GLY114*, SER115*, LYS134*, ILE160*, PHE245*, GLY281*, ASP282*, ALA303*.
6d	-7.8	-	GLY7*, CYS8*, THR9*, GLU32*, MET33*, ASN34*, THR112*, THR113*, GLY114*, SER115*, CYS116***, PRO117***, LEU132**, LYS134***, ASN135*, ASP138*, ASN248*.
REF	-8.1	THR9*, HIS10*, GLU32*, VAL81**	VAL6*, GLY7*, ALA11*, GLY12*, TYR31*, MET33**, ASN34*, HIS79*, GLN80*, THR112*, THR113*, GLY114*, SER115*, LYS134*, ASN248*, LEU251*, GLY281*, ASP282*, SER283*, ALA300*, ALA303*.

:** one bond, *:** two bonds, *****:** three bonds, **-:** no interaction bond, **REF:** Adenosine-5'-diphosphate

Prediction of drug-likeness descriptors and toxicity

Prediction of the physico-chemical properties and drug-likeness

Driven by the Molecular Docking outcomes, the physicochemical and pharmacokinetic parameters that determine the ADMET (Absorption, Distribution, Metabolism, Excretion, and Toxicity) criteria were simulated on the selected compounds. The results summarized in Table S2 (supporting information) demonstrate that all tested compounds are in full accordance with Lipinski rule, indicating strong absorption and penetration through the cell membrane, whereas Adenosine-5'-diphosphate did not fulfill this condition. In fact, all the tested compounds presented Log (P) values under five, indicating excellent permeability through the cell membrane. Additionally, the numbers of hydrogen bond donors (nHD) and acceptors (nHA) fell within the range of acceptable values, revealing that all of them can be effective in establishing hydrogen bonds, demonstrating their stability inside the target protein's active site, except for the reference ligand, which presented number of hydrogen bond acceptors and donors beyond the accepted values. Moreover, the Veber rule was adopted for all compounds, allowing them to be bioavailable; this is also presented in the bioavailability radar chart (Figure 3), which indicated that all ligands are virtually completely shifted into the pink zone, indicating their higher oral bioavailability and resemblance to drugs.



6a **6b** **Ref**

Figure 3. Bioavailability radar chart for synthesized compounds. LIPO (lipophilic): − 0.7 < XLOGP3 < 5.0, SIZE: 150 g/mol < MV < 500 g/ mol, POLAR (polarity): 20 Å2 < TPSA < 130 Å2, INSOLU (insolubility): − 6 < Log S (ESOL) < 0, INSATU (insaturation): 0.25 < Csp3 fraction < 1, FLEX (flexibility): 0 < Number of obligatory rotations < 9.

Prediction of pharmacokinetic properties

The medication molecules need to pass through the digestive system and reach the systemic circulation in sufficient amounts. Therefore, it is crucial to comprehend the processes and variables influencing gastrointestinal absorption and metabolism while developing novel medications. In this context, the pharmacokinetic properties of the selected compound were estimated theoretically, and the results are presented in Table S3 (supporting information). The results indicate that **6a** and **6b** had high gastrointestinal absorption (GI), showing high bioavailability, which suggests that a significant portion of the provided dose can be absorbed easily into systemic circulation, unlike the reference, which cannot penetrate the system effectively. Additionally, the selected compounds possessed the capacity to cross the blood-brain barrier (BBB), suggesting that they ought to have an impact on the central nervous system, making them prospective candidates for treating neurological or mental disorders. Moreover, drug-type compounds must not be P-gp (glycoprotein type P) substrates, and all investigated compounds satisfied these criteria, presenting the ability to interact with these cytochromes CYP1A2, CYP2C19, CYP2C9, and CYP3A4. Finally, our data point to a highly promising chemical that fulfills the key pharmacokinetic and safety features necessary for effective medical therapies.

Toxicity analysis

Determining a compound's toxicity is another crucial aspect of the drug design process. Toxic amounts can be determined using computational approaches for toxicity evaluation. Consequently, this makes progress in lowering the probability of failure. On this path, toxicity parameters such as mutagenicity and carcinogenicity of the selected ligands were predicted, and the results are presented in Table S4 (supporting information). The results indicate that the chosen compounds displayed non-mutagenic impact through the Ames test, delivering a lower probability of genetic damage and attractive candidates for further research. Also, **6a** and **6b** presented a negative rat oral acute toxicity test, referring to their safe profiles and probability of proceeding to a later stage of testing. Finally, the selected compounds showed a low risk of hERG inhibition and no carcinogenic effect, proving their low cardiotoxic risks and low potential to cause cancer.

DFT study

Conceptual DFT is a key feature of the density functional programming language that helps clarify and explain the molecular structure and its reactivity [32]. However, quantitative structure-activity relationship (QSAR) investigations in biochemistry have made extensive use of quantum-chemical descriptors. In this regard, the physicochemical parameters of the most active compounds **6a** and **6b** were listed in Table 4 to support and validate the molecular docking findings. They characterize the reactivity of the studied compounds and contribute to clarifying the impact of various substituents on the selected molecules, influencing their stability, depicting their reactivity, and regulating their biological interactions, including how they interact with specific enzymes. Among these parameters, the gap energy (EHOMO – ELUMO), hardness (ELUMO- EHOMO)/2), softness (1/η) and the potential (EHOMO + ELUMO) / 2) [33] were determined. The results indicated full agreement with the molecular docking claims. In fact, the HOMO levels of all selected compounds are good nucleophiles since they require not much to give these electrons towards establishing a new bond. Correspondingly, compound 6b presents a slightly higher HOMO value (-5.78 eV) compared to **6a** (-5.054 eV), making it slightly more reactive in nucleophilic interactions with biological enzymes due to the presence of pyridine's nitrogen, the most evident nucleophilic site (1 hydrogen bond with THR9). Conversely, the comparable ELUMO of the two compounds indicates their aptitude to accept electrons, supporting their electrophilicity, which makes it costless to place an electron into such an orbital. Moreover, the gap energy presents an important parameter that displays the chemical hardness-softness, kinetic stability, and reactivity of molecules. In fact, the two compounds revealed smaller gap energy values, demonstrating their electronic stability and making them suitable as harmless biological agents. Otherwise, compound **6b** presents the highest hardness value (1.500 eV), which makes it the most stable compound, reflecting its greater kinetic stability. However, **6a** displayed the highest softness value (0.8eV), which makes it the more reactive compound (3 hydrogen bonds with CYS8, THR9, and SER41). All these results uphold the molecular screening findings.

In the same path, the frontier molecular orbital theory states that the most important components are HOMO and LUMO, as these orbitals serve as indicators of the reactivity and characteristics of molecules. On this path, the repartition and energy levels of the HOMO and LUMO orbitals of the tested compounds are presented in Figure 4. The findings indicate that the HOMO orbital is localized on the pyrazole ring for both **6a** and **6b**. However, except for the isoxazole ring (**6a**) and the pyridine ring (**6b**), the LUMO orbital is mostly concentrated throughout all the structures.

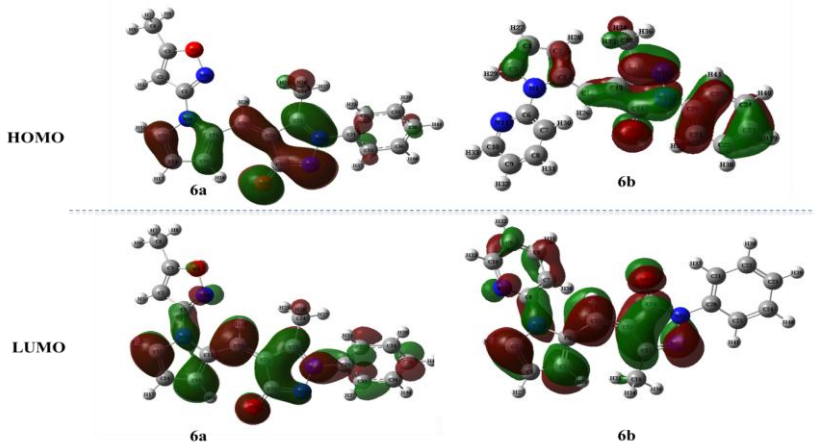


Figure 4. Frontier molecular orbital of selected compounds.

Table 4. The physicochemical descriptors of compounds **6a** and **6b**.

Compound	**6a**	**6b**
E_{HOMO}	-5.054	-5.578
E_{LUMO}	-2.553	-2.577
ΔE	2.501	3.001
S	0.8	0.666
η	1.25	1.5
μ	-3.803	-4.077

E_{HOMO}: Energy of the orbital HOMO (eV), E_{LUMO}: Energy of the orbital LUMO (eV), ΔE: Gap energy (eV), S: Softness (eV), η: Hardness (eV), μ: Chemical potential (eV).

In order to understand the biological awareness and hydrogen interactions, as well as to interpret electrophilic and hydrophobic bindings, the molecular electrostatic potential (MEP) mappings of the tested compounds are presented in Figure 5. Positive (blue) regions of the MEP indicate electrophilic reactivity (electron deficiency), whereas negative (red and yellow) regions indicate nucleophilic reactivity (electron-rich zones). The MEP of compound **6a** revealed that the negative potential regions (red zones) are localized around the carbonyl group of the pyrazole rings, with some contrast around the oxygen of the isoxazole cycle. These areas are vulnerable to nucleophilic attacks by the free doublet of the oxygen atom, which is demonstrated in the 3 hydrogen interactions with CYS8, SER41, and THR9. Otherwise, the positive potential area for **6a** is concentrated around the hydrogens attached to the pyrrole and isoxazole rings, favoring electrophilic attacks (15 hydrophobic interactions with amino acid residues). For **6b**, the negative potential regions are localized as well around the carbonyl group of the pyrazole rings and the nitrogen of the pyridine cycle, demonstrating that these areas are favorable for nucleophilic attack (2 hydrogen bonds with THR9 and SER41). Likewise, the blue zone is also localized around the hydrogen attached to the pyrrole and the pyridine rings.

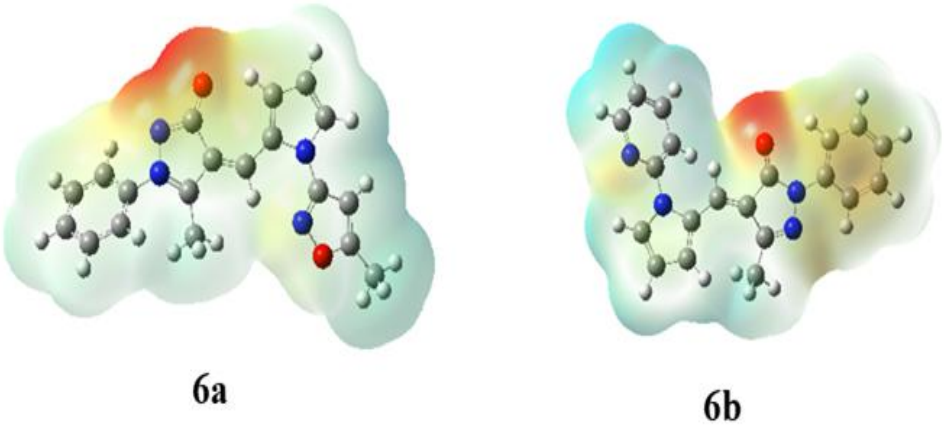


Figure 5. Molecular electrostatic potential of selected compounds.

CONCLUSION

In this study, new pyrrole derivatives were synthesized via the Clauson class reaction. Then, formyl pyrroles were synthesized, and their reactivity toward two different activated methylenes was studied in order to synthesize unsaturated compounds, which were characterized by DRX, FT-IR, and ^{1}H and ^{13}C-NMR spectral techniques. The antioxidant potential of these molecules was predicted in silico, as well as their ADMET profiles. The results indicated that some candidates (**6a** and **6b**) may serve as antioxidant agents. Finally, the characterization of the structural proprieties has been explored theoretically using density functional theory (DFT). In general, these findings provided evidence for the promise the synthesized pyrrole scaffolds offer for the development of antioxidant reagents. Further work will be devoted to their experimental *in vitro* and *in vivo* validation.

ACKNOWLEDGEMENTS

This work was financially supported by the Tunisian Ministry of Higher Education and Scientific Research.

Declarations

Conflict of Interest: The authors declare that they have no known competing financial interests or personal relationships that could have appeared to influence the work reported in this paper.

Ethical approval: Not applicable.

Informed consent: Not applicable.

Data availability

All data generated or analyzed during this study are included in this published article and its supporting information. Crystallographic data are available from the CCDC (deposition numbers 2420575 and 2478473.

REFERENCES

1. Parab, A.; Dawda, H.; Mukundan, U. A review of reactive oxygen species (ros) in plants. *J. Adv. Sci. Res.* **2023**, 14, 1-7.
2. Sachdev, S.; Ansari, S.A.; Ansari, MI. *Reactive Oxygen Species (ROS): An Introduction. In: eds. Reactive Oxygen Species in Plants: The Right Balance*, *Springer Nature Singapore Pte Ltd*; **2023**; p.1-22.
3. Touyz, R.M.; Camargo, L. *Reactive oxygen species and oxidative stress, In Primer on the Autonomic Nervous System*, 4th ed., Academic Press; **2023**; p 345-352.
4. Yiran, D.; Jiayi, W.; Lifang, M. *Harnessing Antioxidants to Counter Oxidative Stress-Induced Apoptosis. In: The Power of Antioxidants - Unleashing Nature's Defense Against Oxidative Stress*. IntechOpen, **2024**; p 1-15.
5. Xie, W.; Wiriyarattanakul, S.; Rungrotmongkol, T.; Shi, L.; Wiriyarattanakul, A.; Maitarad, P. Rational design of a low-data regime of pyrrole antioxidants for radical scavenging activities using quantum chemical descriptors and QSAR with the GA-MLR and ANN concepts. *Molecules* **2023**, 28, 1596-16111.
6. Javid, H.; Moghadam, E.S.; Farahmandfar, M. Biological activity of novel pyrrole derivatives as antioxidant agents against 6-OHDA induced neurotoxicity in PC12 Cells. *Iran. J. Pharm. Res.* **2023**, 22, e140450.

7. Fatahala, S.S.; Shalaby, E.A; Kassab, S.E; Sayed Mohamed, M. A promising anti-cancer and anti-oxidant agents based on the pyrrole and fused pyrrole: Synthesis, docking studies and biological evaluation. *Anticancer Agents Med. Chem.* **2015**, 15, 517-526
8. Nguyen, T.; Dai, V.V; Mechler, A.; Meervelt, L.V; Thi Hoad, T.; Quan, V.Vo. Synthesis and computational evaluation of the antioxidant activity of pyrrolo[2,3-b]quinoxaline derivatives. *RSC Adv.* **2024**, 34, 24438-24446.
9. Mateev, E.; Georgieva, M.; Zlatkov, A. Design, microwave-assisted synthesis, biological evaluation, molecular docking and ADME studies of pyrrole-based hydrazide-hydrazones as potential antioxidant agents. *Maced. J. Chem. Chem. Eng*. **2022**, 41,175-186.
10. Sheldrick, G.M. A short history of *SHELX*. *Acta Crystallogr. A* **2008**, 64, 112-122.
11. Sheldrick, G.M. Crystal structure refinement with SHELXL. *Acta Crystallogr Sect. C. Struct. Chem.* **2015**, 71, 3-8.
12. X-Ray Diffraction | X-Ray Diffraction Instrumentation | Thermo Fisher Scientific - TN. Accessed: Sep. 12, **2025**.
13. Macrae, C.F.; Sovago, I.; Cottrell, S.J. Mercury 4.0: From visualization to analysis, design and prediction. *J. Appl. Crystallogr.* **2020**, 53, 226-235.
14. Farrugia, L.J. WinGX and ORTEP for Windows: An update. *J. Appl. Crystallogr*. **2012**, 45, 849-854.
15. Trott, O.; Olson, A.J. AutoDock Vina: Improving the speed and accuracy of docking with a new scoring function, efficient optimization, and multithreading. *J. Comput. Chem*. **2010**, 31, 455-461.
16. Frisch, M. Gaussian 09, Revision d. 01, Gaussian. *Inc Wallingford CT*, 201, 2009, Accessed: Jul. 22, 2024. [Online]. Available: https://cir.nii.ac.jp/crid/1370298757422456580.
17. Dennington. GaussView, version 5 - Google Scholar. Accessed: Jul. 22, **2024**.
18. Mir, R.H.; Mir, P.A.; Roohi M.; Saba, S.; Mudasir, M.; Shah, A.J; Shenmar, K.; Raza, S.N; Pottoo, F.H. A comprehensive review on journey of pyrrole scaffold against multiple therapeutic targets. *Anticancer Agents Med. Chem.* **2022**, 22, 3291-3303.
19. Sahu, B.; Sahu, R.; Gidwani, B.; Mishra, A. Pyrrole: An Essential framework in the development of therapeutic agents and insightful analysis of structure-active relationships. *Chemistryselect* **2024**, 9, e202401604.
20. Ganesh, B.H.; Raj, A.G.; Aruchamy, B.; Nanjan, P.; Drago, C.; Ramani, P. Pyrrole: A decisive scaffold for the development of therapeutic agents and structure-activity relationship. *ChemMedChem.* **2024**, 19, e202300447-e202300447.
21. Idhayadhulla, A.; Kumar, R.S; Nasser, A.A; Manilal, A. Synthesis and antimicrobial activity of some new pyrrole derivatives. *Bull. Chem. Soc. Ethiop.***2012**, 26, 429-435
22. Marvi, O.; Nahzomi, H.T. Grinding solvent-free Paal-Knorr pyrrole synthesis on smectites as recyclable and green catalysts. *Bull. Chem. Soc. Ethiop.***2018**, 32, 139-147.
23. Gullapelli, K.; Brahmeshwari, G.; Ravichander, M. A facile synthesis of 1-aryl pyrroles by Clauson-Kaas reaction using oxone as a catalyst under microwave irradiation. *Bull. Chem. Soc. Ethiop.* **2019**, 33, 143-148.
24. Miles, K.C.; Mays, S.M.; Southerland, B.K.; Auvil, T.J.; Ketcha, D.M. The Clauson-Kaas pyrrole synthesis under microwave irradiation. *Arkivoc*. **2009**, 14, 181-190.
25. Sheriff Shah, S.K.; Kumar Singh, A.; Banerjee, S.; Singha, T.; V Nair, A.; Ojha, M.; Mondal, A.; Kumar Datta, P.; Pradeep Singh, N.D. Dihydropyrrolo[3,2-b]pyrrole-3,6-dicarbaldehyde-based two-photon-responsive nanoparticles for effective photodynamic therapy. *ACS Appl. Nano. Mater.* **2022**, 5, 9594-9603.
26. Kurihara, T.; Sakamoto, Y.; Kobayashi, T.; Mori, M. The Knoevenagel condensation of ethyl acylpyruvates. *J. Heterocycl. Chem.* **1978**, 15, 737-743.
27. Tarafdar, A.; Pula, G. The role of NADPH oxidases and oxidative stress in neurodegenerative disorders. *Int. J. Mol. Sci.* **2018**, 19, 3824-3843.

28. Wang, Y.; Liu, Q.; Zhao, W.; Zhou, X.; Miao, G.; Sun, C.; Zhang, H. NADPH oxidase activation contributes to heavy ion irradiation-induced cell death. *Dose-Response*. **2017**, 15, 1-6.
29. Da Silva, C.J.; da Silva, R.R.; da Silva, L.C.K.; do Socorro, B.D.; Henrique Tomich de Paula da Silva, C.; Figueiredo Batista Ferreira, E.; dos Santos Borges, R.; Campos, M.J.; da Cruz Macêdo, J.W.; dos Santos, B.R.C. An in silico study of the antioxidant ability for two caffeine analogs using molecular docking and quantum chemical methods. *Molecules* **2018**, 23, 2801-2818.
30. Vadabingi, N.; Avula, V.K.R.; Zyryanov, G.V. Multiple molecular targets mediated antioxidant activity, molecular docking, ADMET, QSAR and bioactivity studies of halo substituted urea derivatives of α-Methyl-l-DOPA. *Bioorg. Chem.* **2020**, 97, 103708-103728.
31. Kohn, W.; Becke, A.D.; Parr, R.G. Density functional theory of electronic structure. *J. Phys. Chem.* **1996**, 100, 12974-12980.
32. Parr, R.G.; Yang, W. Density functional approach to the frontier-electron theory of chemical reactivity. *J. Am. Chem. Soc.* **1984**, 106, 4049-4050.
33. Manachou, M.; Gouid, Z.; Almi, Z.; Belaidi, S.; Boughdiri, S.; Hochlaf,M. Pyrazolo[1,5-a][1,3,5]triazin-2-thioxo-4-ones derivatives as thymidine phosphorylase inhibitors: Structure, drug-like calculations and quantitative structure-activity relationships (QSAR) modeling. *J. Mol. Struct.* **2020**, 1199, 127027-127036.